Panel Movement Effects on Solution Flow in Through-Holes of Printed Circuit Panels

A hydrodynamic model is developed relating the movement of printed circuit panels to solution flow in through-holes. Qualitative and quantitative model verification is experimentally established. Effects of external gas bubbling on hole solution transport are elucidated. Based on the hydrodynamic model, panel motion criteria for contamination-free and fast chemical processing are introduced. Limits of mechanical panel movement as a method for processing holes of different geometry with typical wet chemical process baths are addressed.

R. T. Galasco, A. P. David, and R. R. Shaffer
I. B. M. Development Laboratory
Endicott, NY 13760

Introduction

Fabrication of multilayer printed circuit panels involves a large number of chemical processing operations. Each chemical process operates on one or more of three different geometry scales of the panel (Kessler and Alkire, 1976 a, b). The macroscale geometry refers to the length and width dimension of the front and back surfaces of the panel (typical measurement magnitude 10^{-1}–10^{-2} m). The microscale geometry is specific to the topography of the panel surfaces (e.g., roughness dimensions about 10^{-6} m). The miniscale geometry has measurement dimensions between the macro- and microscale geometries (measurement magnitude 10^{-3}–10^{-4} m). This geometry results from the circuitization of the panel; typical features are circuit lines and pads, blind vias, and plated through-holes.

Plated through-holes (PTH) are present to provide electrical connections among the different circuit layers of a panel. During processing a typical panel drilled with thousands of these holes is exposed to a large number of wet chemical process operations. Oscillating panel motion is required to provide solution transport in the PTH (Schering/Chemcut; Heikkla et al., 1984). In some cases, the PTH solution flow is disturbed by gas sparging and/or solution pumping in the bulk solution for mixing (Malak 1981; Tidwell et al.). Inadequate PTH solution flow will cause processing problems yielding scrap product. Also, mixing of different chemical baths can occur, reducing bath lifetime and increasing process cost.

Haak et al. (1981) studied mass transfer in PTH by measuring limiting current densities. Mass transport ratios were reported for different gas bubble rates and low reciprocating panel movement. Some volumetric solution flow rates in the PTH were given. Ju (1984) investigated both mass transfer and fluid flow for a stationary PTH with an impinging solution jet. The present paper deals with the PTH solution flow resulting from the reciprocating panel motion typical for printed circuit panel processing. A hydrodynamic model is introduced relating the solution velocity in the PTH miniscale geometry to the macroscale motion of the panel. Qualitative and quantitative model verification is established experimentally. Effects of bulk solution flow induced by gas bubbling on PTH solution flow patterns are also experimentally investigated. Model application is performed to provide panel motion criteria for contamination-free and fast chemical processing. Limits of reciprocating panel motion for processing holes of different geometry with various solutions are discussed.

Hydrodynamic Model

Consider the horizontal motion of a porous flat plate or panel through a solution in a process tank. Fluid displacement occurs from the panel front around the edges and through the holes, Figure 1. The flow around the edges will be unrestricted if sufficient clearance is allowed between the panel and process tank sides and bottom, and between the panel and solution surface level (for an open-top tank). Neglecting any secondary solution flow due to solution recirculation or gas sparging, the primary flow field is caused by panel motion. Since the panel cross-sectional area (macroscale geometry) is large relative to panel thickness and porosity dimensions (miniscale geometry), the pressure drop for flow around the panel edges can be determined from a drag coefficient relation (Binder, 1959)

$$\Delta P_P = \frac{C_D \rho V_P^2}{2} \tag{1}$$

where ΔP_P is the pressure drop across the board, C_D is the drag coefficient, ρ is the fluid mass density, and V_P is the panel velocity.

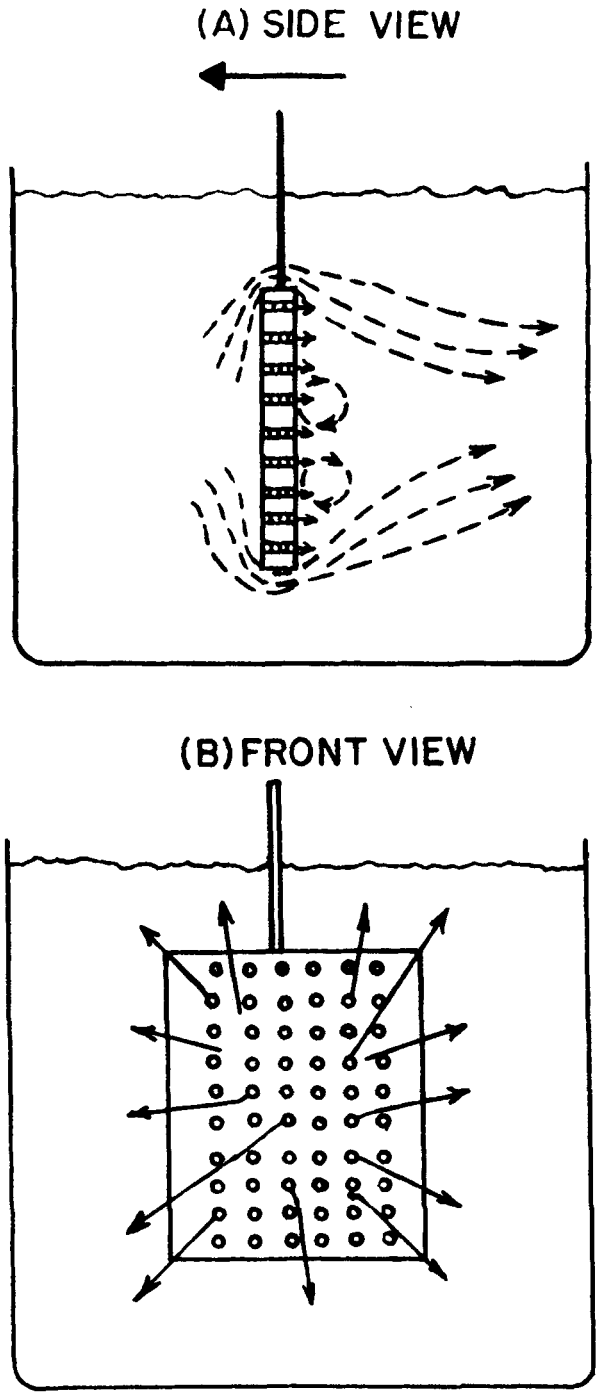

Figure 1. Fluid flow around a moving printed circuit panel.

Solution flow in the holes is expected to be laminar in nature. To determine if entry losses and transition effects to a fully developed boundary layer are negligible, a flow factor for fully developed flow profile (Langhaar, 1942) can be applied

$$\frac{4L}{(N_R)_H D} > 0.12 \tag{2}$$

where L/D is the aspect ratio of the hole and $(N_R)_H$ is the hole Reynolds number. For flow factors greater than 0.12 (high aspect ratios with low flow rates), fluid flow in the hole is laminar with a fully developed boundary layer, Figure 2. The pressure flow relationship can be determined by the Hagen-Poiseuille law (McCabe and Smith, 1957)

$$\Delta P_H = \frac{32\mu L V_H}{D^2} \tag{3}$$

where ΔP_H is the pressure drop across the hole, μ is the dynamic viscosity, and V_H is the solution velocity in the hole. For flow factors less than 0.12 (low aspect ratios with high flow rates), a more general pressure flow relationship for developing laminar flow must be applied

$$\Delta P_H = 1.142\,\rho V_H^2 + \frac{32\mu L V_H}{D^2} - \frac{0.642\,\rho V_H^2}{1 + \dfrac{215.6\,L\mu}{D^2 \rho V_H} + 5.26 \times 10^6 \left(\dfrac{L\mu}{D^2 \rho V_H}\right)^4} \tag{4}$$

This relationship was established by empirical fitting of Langhaar's theory for developing flow in short tubes (Pimbley, 1982). In the regime of high flow factors (more commonly encountered in circuit panel applications) this relation reduces to the Hagen-Poiseuille law.

The hydrodynamic model results from the allowance of one-dimensional pressure variation in the solution. Thus, the pressure drops across the panel resulting from flow around the panel edges, Eq. 1, and flow through the holes, Eq. 3 or 4, can be equated. For fully developed laminar flow in the holes, the solution hole velocity is related to panel velocity by

$$V_H = \frac{C_D D^2 V_P^2}{64\,L\eta} \tag{5}$$

This relationship includes the effects of panel dimensions and fluid properties on the fluid hole and panel velocities. A similar but more cumbersome relation can be obtained for a hole flow condition of developing laminar flow.

Hydrodynamic model calculations of solution flow in holes for typical circuit panel processing conditions are given in Table 1. Low Reynolds numbers for solution transport in the hole imply laminar flow. The range of flow factor criterion values indicates that both fully developed and undeveloped flows are achievable, although the former situation is more likely. Total fluid flow around the panel edge is determined from a volume balance of the incompressible fluid. This flow is equivalent to the total fluid dispersed by panel motion reduced by the volumetric flow rate in the holes. By comparison, most of the displaced fluid flows around the panel edges. This flow is primarily responsible for the pressure drop across the panel. High Reynolds numbers dictate that the flow is generally turbulent, with a turbulent wake behind the panel. In this flow regime, the panel drag coefficient remains relatively constant and depends only on panel length and width dimensions (Eisher, 1981).

Experimental Method

Flow visualization studies

Flow visualization studies were undertaken for qualitative verification of the hydrodynamic model. The experimental ap-

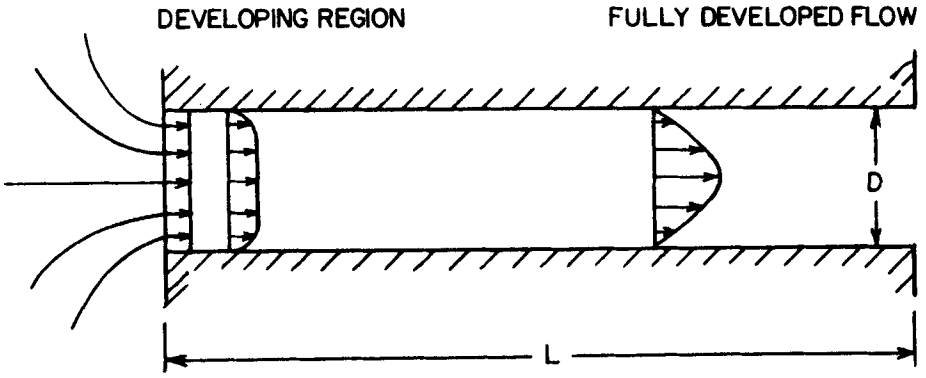

Figure 2. Develping and fully developed flow in a through-hole.

paratus consisted of transparent polyethylene tanks with Lucite panel models. Clear tank solutions were injected with dye or air bubbles to make fluid flow characteristics visible. A video cassette recorder was used to obtain permanent records of the experiments. In all cases, reciprocating panel motion of constant velocity was studied. This motion was maintained by panel connection to a lead screw driven by a stepping motor. Stepping motor operation was controlled by a modified Superior Preset Indexer (model SP 153A).

Scaled hole studies were performed in a rectangular tank containing a panel model with a single smooth hole. To aid visual observation of solution flow in the hole, the hole dimensions were scaled 20 times larger than a typical circuit panel hole of 0.4 cm dia. with a 9.4 aspect ratio. Flow similarity was maintained by using a high-viscosity glycerin with 20 times H_2O viscosity to hold the hole Reynolds number constant (Bird et al., 1960). Air bubbles, oil-soluble dyes, and insoluble dyes were injected into the glycerin with a syringe. To simulate typical topography for a drilled hole, a continuous spiral of epoxy was positioned on the hole wall.

Fluid flow external to the panel was studied in a 15 L process tank containing deionized water. A 5.1 cm × 7.6 cm panel model with 720 holes of 0.40 cm dia. (aspect ratio = 9.4) was immersed in the tank. This panel model represents a typical section of an actual printed circuit product. Hypodermic needles were mounted on the external front and back surfaces of the panel. During flow visualization testing, these needles injected a water-soluble dye into the bulk solution. Dye injection rates were controlled by a pneumatic regulator system designed in our laboratory.

Table 1. Typical Range of Panel Dimensions and Solution Flow Parameters for Circuit Panel Processing

L_P = 25 cm
W_P = 38 cm
N_H = 10,000–30,000
D = 0.046–0.102 cm
L = 0.102–0.408 cm
η = 0.0045–0.0129 cm²/s
V_H = 0.007–9.7 cm/s
$(N_R)_H$ = 0.025–220
$\frac{4L}{(N_R)_H D}$ = 0.018–1,600
Q_H = 1.2–150 cm³/min
Q_P = 950–4,600 cm³/min
V_P = 1.0–5.0 cm/s
$(N_R)_P$ = 2,000–40,000

Shear stress measurements

Quantitative model verification was performed by measuring average solution hole velocities for different panel movement rates. For fully developed laminar flow in a hole the average solution velocity V_H is obtained from

$$V_H = \frac{D\tau_w}{8\mu} \tag{6}$$

where τ_w is the wall shear stress. The wall shear stress was measured experimentally by the electrochemical method developed by Hanratty (Dimopoulos and Hanratty, 1968; Muzushina, 1971; Hanratty and Campbell, 1983). In this method, small electrodes are imbedded into the wall of a hole. The electrode dimension in the direction of fluid flow must be small relative to hole curvature so that a two-dimensional concentration boundary layer can be assumed. Aqueous solution transport in the hole is characterized by a large Schmidt number (small mass transfer boundary layer) and Peclet number (large convection relative to diffusion in flow dimension). For steady state conditions, the wall shear stress can be determined with measurements of diffusion D_i and mass transfer K coefficients from the relation

$$\tau_W = 1.90 \frac{\mu K^3 L_E}{D_i^2} \tag{7}$$

where L_E is the electrode length in flow direction.

0.032 M potassium ferricyanide and 0.032 M potassium ferrocyanide in 1.0 M sodium hydroxide was chosen as the soluble product and reactant redox couple for experimental studies

Table 2. Physical Properties of Potassium Ferricyanide/Ferrocyanide Redox Couple System

n_e = 1
D_i = 5.8 × 10⁻⁶ cm²/s
η = 0.0124 cm²/s
ρ = 1.062 g/cm³
μ = 0.0132 g/cm · s
T = 298 K
S_C = 2,140

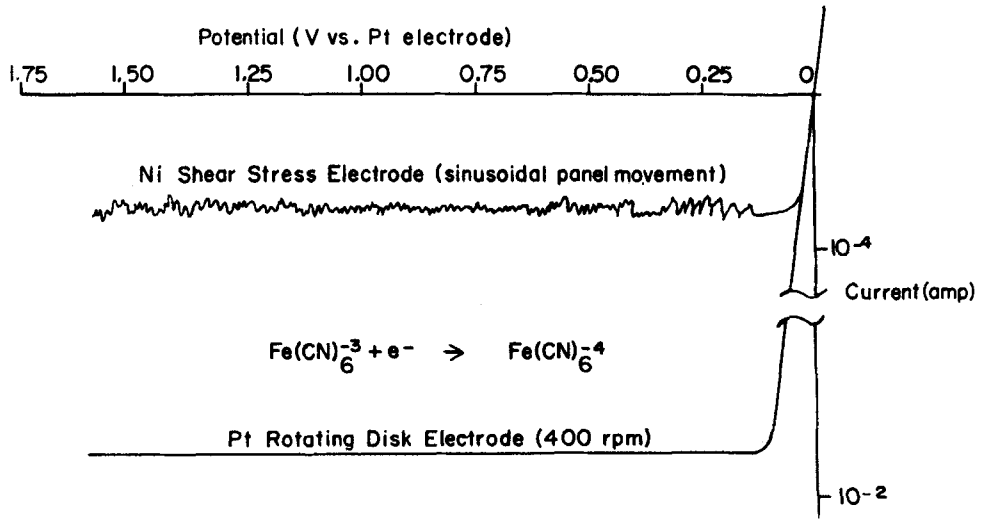

Figure 3. Limiting current plateau for ferricyanide/ferrocynanide system.

(Selman and Tobias, 1978; Alkire and Chen, 1982). This couple has been studied extensively by electrochemists, and the physical properties, including the diffusion coefficient, are easily measured or readily available in the literature; the properties are listed in Table 2. Mass transfer coefficients were determined from limiting current i_L measurements with the relation (Selman and Tobias, 1978)

$$K = \frac{i_L}{n_E F C_B} \tag{8}$$

where C_B is the bulk ferricyanide concentration. A typical polarization curve for the reduction of ferri- to ferrocyanide is given in Figure 3. During limiting current measurement, working electrodes were held at the mid-potential in the limiting current plateau.

Test vehicles were 5.08 cm squares with a single drilled hole in the center. Each hole contained three nickel electrodes separated with insulating material, Figure 4. The insulating material was composite, consisting of polyimide separator coated with a Torrseal epoxy. To avoid chemical attack, no polyimide was exposed to the test solution. Measurements of the three electrodes varied less than 25% and average values were utilized for data analysis. Upon test completion a cross section of each hole was examined with a light microscope and true nickel areas were determined.

Test vehicles were submerged approximately 2.54 cm below the solution level in a 10.2 cm × 30.5 cm rectangular cell of 15.2 cm depth. A platinum wire of 0.081 cm dia. was positioned on one cell face to act as a counterelectrode. A platinum ring was mounted on the test vehicle surface opposite the counter electrode. This platinum ring was centered around the hole and acted as a reference electrode. Reciprocating vehicle movement with a sinusoidal velocity shape was studied. This motion was maintained by linear translation of rotational motion of an electric motor. When required, nitrogen bubbles were introduced

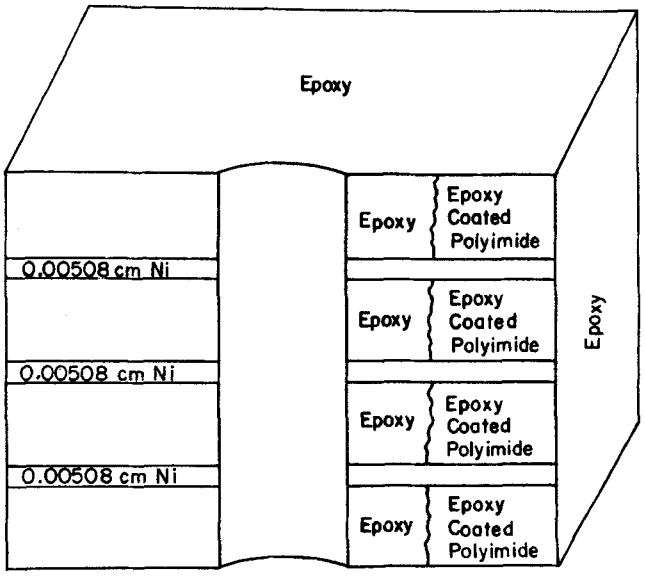

Figure 4. Test vehicle construction for mass transfer coefficient measurements.

into the solution via a sparger tube along the cell bottom. Gas flow rate was controlled by a Fischer flowmeter (model 11-163-75A). The data acquisition system is illustrated in Figure 5. Prior to testing, dissolved oxygen was removed from solution via nitrogen bubbling for 4 h at 0.14 std $cm^3/s \cdot cm^2$. Also, the nickel electrodes were reduced at 20 $mamp/cm^2$ in a solution of 1 M sodium hydroxide to eliminate potential fouling problems at the electrode surface with nickel cyanide. To avoid oxygen redissolution during testing, the pressurized nitrogen atmosphere was always maintained above the solution surface.

Results

Flow visualization studies

Initially, oil-soluble dye was placed in the scaled hole to observe fluid motion for different panel movement rates. Fully developed laminar flow was identified with a parabolic velocity profile. At low panel velocities the dye oscillated in the center of the hole. With increasing panel velocities, enhanced fluid displacement occurred, eventually resulting in dye ejection from the hole. Similar phenomena were observed with both smooth and rough holes.

Contamination effects were investigated by injection of air bubbles and high-density insoluble dye droplets into the hole center. Due to buoyant forces, the air bubbles always attached to the top surface of the hole. The dye took residence at the hole bottom because of gravity effects. With inadequate panel movement, the contaminants oscillated back and forth but were not removed. At high panel velocities, contaminant removal was easily accomplished.

Fluid flow patterns external to the panel were examined by dye injections at the surface of the printed circuit panel model. During movement, the majority of the fluid displaced by the panel traveled around the edges. A resulting turbulent wake was formed behind the panel due to boundary-layer separation. At higher panel velocities, the amplitude and persistence of the turbulent wake increased. For extremely rapid panel movement, the turbulent wake did not dissipate before the panel changed direction and passed through the wake area. Movement in the eddies caused pressure distribution fluctuations across the panel. The flow pattern in the holes was altered in a manner not easy to determine. To break up solution eddies prior to panel motion through the wake area, flow straighteners (screens) were located on either side of the panel.

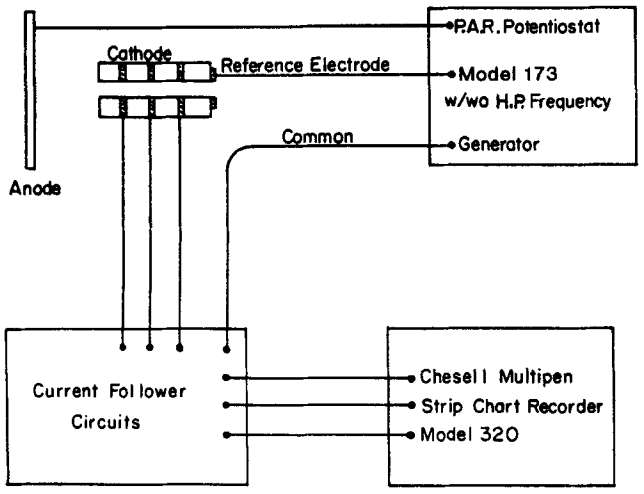

Figure 5. Data acquisition system for mass transfer coefficient measurements.

Table 3. Hole Dimensions of Vehicles for Shear Stress Testing

Vehicle	Hole Dia. cm	Vehicle Thickness cm	Aspect Ratio
1	0.0348	0.345	9.91
2	0.0450	0.353	7.84
3	0.0450	0.227	5.02
4	0.0752	0.345	4.59
5	0.366	0.358	0.98

Shear stress measurements

Solution velocities were measured for holes varying one order of magnitude in aspect ratio; hole dimensions are given in Table 3. Average panel velocities from 1.27 to 19.05 cm/s were achieved by variation of panel stroke X_p and displacement rate n. Generally, hole solution velocities varied sinusoidally with time at the same frequency as panel velocities. Due to interaction of the pressure fields between forward and reverse panel motion, maximum solution velocities were not always equivalent in magnitude, Figure 6. Minimum solution velocities never reached zero because of constant solution flow induced by the continuous panel movement and/or cell boundary effects. Typically, amplitude ranges for solution hole velocities varied over a

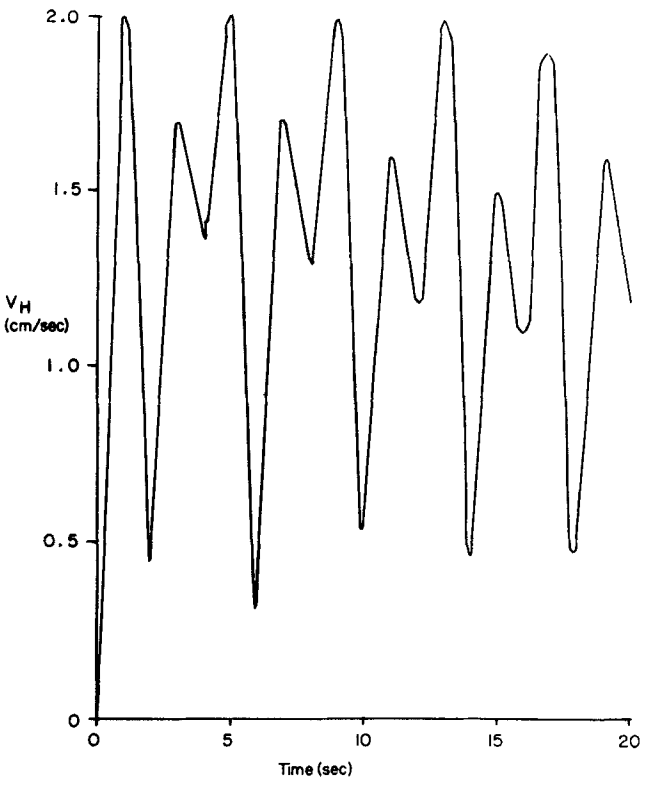

Figure 6. Solution hole velocities resulting from sinusoidal panel movement.
D = 0.0450 cm; L/D = 5.02; n = 15 cycle/min; X_p = 7.62 cm

wide band relative to the average velocities, Figure 7. This wide variability can be greatly diminished by use of a panel movement system (e.g., lead screw with stepping motor) for ramping velocities.

Quantitative model verification was approached by comparison of experimentally measured average solution velocities with hydrodynamic model predictions at average panel velocities. Utilizing a correlation for undirectional flow around a flat plate, the hydrodynamic model predictions are of the same order of magnitude but lower than experimental data, Figure 8. The discrepancy in magnitude is caused from the drag coefficient, which does not account for sinusoidal velocity profiles, cell boundary effects, and continuously reversing solution flow. An excellent fit to the model is achieved by utilizing the experimental data to determine the characteristic drag coefficient for the system (C_D = 2.1). This good fit is consistently observed for solution velocities varying three orders of magnitude, Figures 8–10. For the large-diameter hole of low aspect ratio, turbulent solution flow in the hole occurred at higher panel velocities. This flow regime is outside the application range of the hydrodynamic model. Also, average hole solution velocities for this type of flow cannot be determined from experimental data using Eq. 6.

The effect of gas bubbling in the bulk solution on fluid transport in the hole was also investigated. The range of gas bubbling rates was fixed to provide vigorous bulk solution agitation without severe surface splashing or potential solution spillage. For a stationary panel, a constant stream of gas bubbles on both panel sides induces low solution flow rates in the holes, Table 4. This

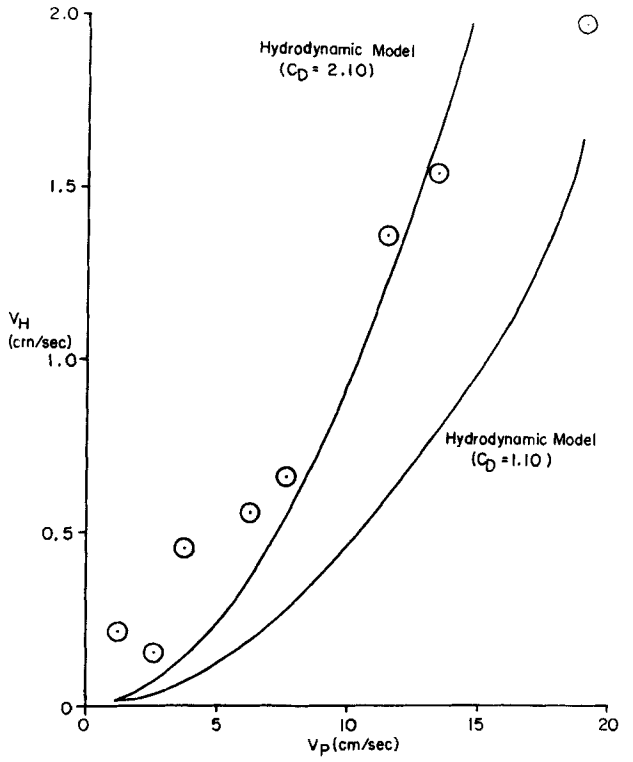

Figure 8. Comparison of predicted and measured solution hole velocities.
D = 0.0348 cm; L/D = 9.91

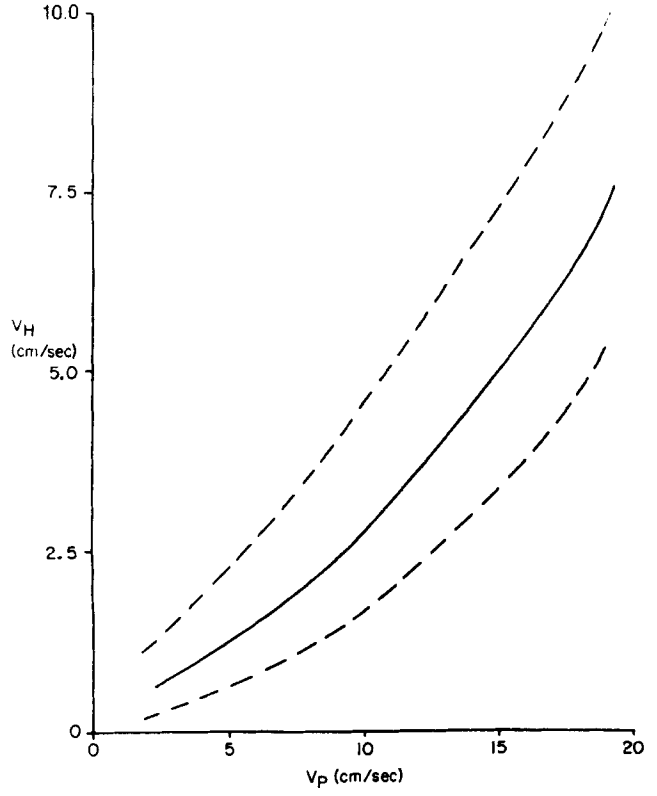

Figure 7. Typical amplitude range for solution hole velocities.
D = 0.0450 cm; L/D = 5.02

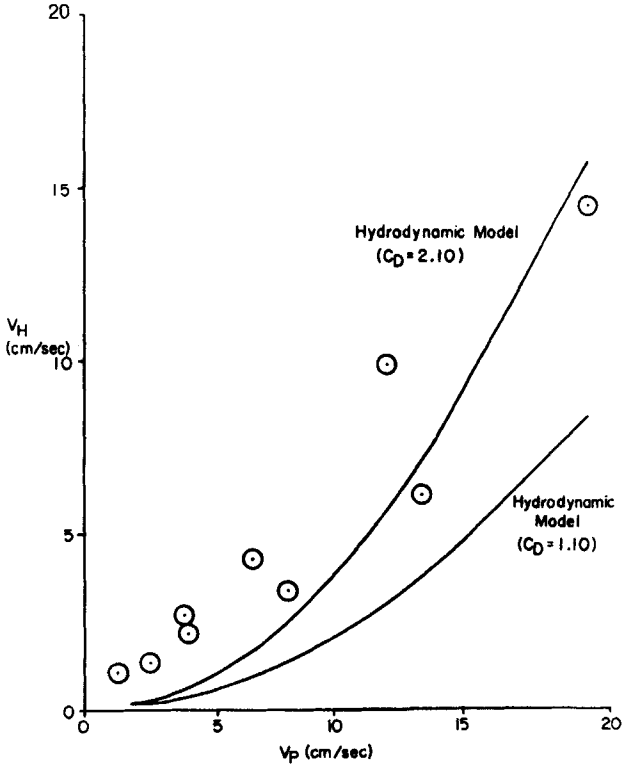

Figure 9. Comparison of predicted and measured solution hole velocities.
D = 0.0752 cm; L/D = 4.59

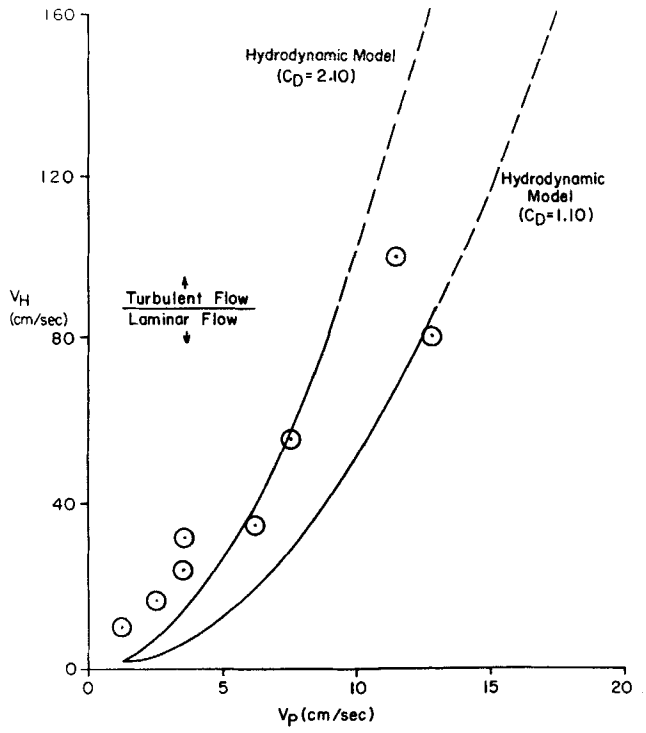

Figure 10. Comparison of predicted and measured solution hole velocities.
D = 0.366 cm; L/D = 0.98

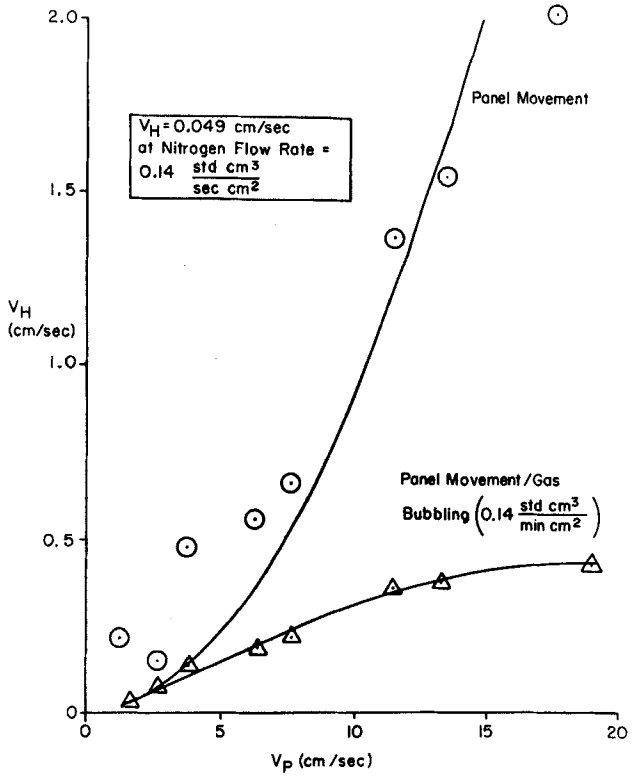

Figure 11. Effect of panel motion/gas bubbling on solution hole velocity.
D = 0.0348 cm; L/D = 9.91

solution flow is caused by localized variation of the pressure drop at opposite ends of the hole. Unbalanced bubble flow from panel side to side can yield this pressure drop. Pressure variabilities may also occur because of bubble blockage of solution transport at the hole surface followed by solution entrainment from the hole in the wake of rising bubbles. Regardless of the flow mechanism, uniform gas bubbling external to the panel yields much smaller solution flow rates in holes than does panel movement.

Superimposing gas bubbling with panel movement significantly reduces hole solution transport relative to panel motion alone, Figures 11 and 12. The uniform gas bubbling on both sides of the panel breaks up the pressure field generated by panel movement for fluid flow. A similar detrimental effect on hole solution transport will probably take place with panel movement through its own turbulent wake. From flow visualization studies, this situation can occur at very high panel velocities with oscillating panel movement.

Haak et al. (1981) reported volumetric solution flow rates in

Table 4. Solution Flow in Through-Holes Induced by Gas Bubbling*

Hole Aspect Ratio	Induced Hole Solution Flow (cm/s) from	
	Gas Bubbling	Panel Movement
9.91	0.0128–0.0591	0.211–2.00
4.59	0.141–0.565	1.08–14.6
0.98	3.15–6.78	10.9–101

*Bubbling rate 0.03–0.27 std $cm^3/s \cdot cm^2$

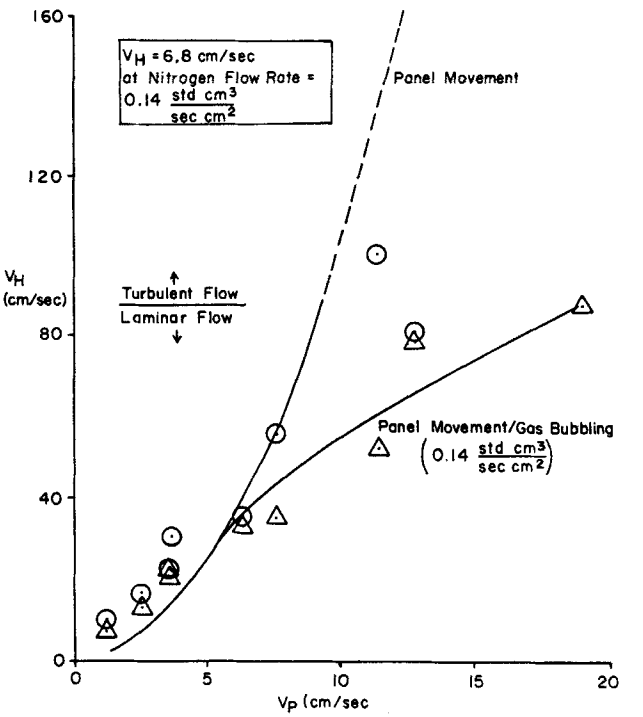

Figure 12. Effect of panel motion/gas bubbling on solution hole velocity.
D = 0.366 cm; L/D = 0.98

PTH at a low panel velocity of 1.2 cm/s for external gas bubble rates of 0–0.67 std $cm^3/s \cdot cm^2$. Flow was studied in a multiple hole system of 0.12 cm dia. (L/D = 2.67). Conversion of this data into hole solution velocities is difficult since the total cross-sectional area basis of the volumetric flow is unclear. Volumetric solution flow in the holes remained relatively constant for gas flow rates of 0–0.33 std $cm^3/s \cdot cm^2$. These data are consistent with hole solution velocities in our system at a similar low panel velocity. Here, very little difference is found with/without gas bubbling for a low aspect ratio hole, Figure 12. Volumetric solution flow in the holes increased four times to a gas-bubble-induced transport limit when the gas flow rate was doubled to 0.67 std $cm^3/s \cdot cm^2$. Solution hole velocity data under similar conditions were not generated in our studies. However, much higher increases in solution hole velocity were induced by increasing panel movement with/without gas bubbling, Figures 11 and 12.

Discussion

Conventional wet processing of holes in printed circuit panels involves reciprocating panel movement supplemented with a gas bubbling and/or pumped solution recirculation. The shear stress data presented here indicate that gas bubbling with/without panel movement is not generally sufficient to generate reasonable hole fluid transport rates. Therefore, gas sparging external to the process tank is recommended when required for bulk solution mixing or solution oxygenation purposes. If bubbles are generated during processing (e.g., H_2 evolution in baths for electroless copper plating), flow straighteners next to the panel will minimize the effects. Direct testing was not performed on solution recirculation resulting from pumping. For typical low pump rates, minimal impact on hole solution movement is expected. Therefore, mechanical panel movement is the major driving force for solution flow in holes.

Flow visualization studies revealed that low panel movement rates can cause contamination buildup in holes. For contamination-free processing, complete exchange of all fluid in a hole is necessary during each single-direction panel stroke. Complete solution exchange is guaranteed when the hole fluid displacement X_H is equal to or greater than the panel thickness L. Application of this criterion to the hydrodynamic model yields panel agitation requirements from

$$\frac{nX_p^2}{60} \geq 15.2\eta \left(\frac{L}{D}\right)^2 \tag{9}$$

Soluble contaminants (e.g., reaction by-products, solution drag-out) can also be removed from holes by diffusion and mixing mechanisms with adequate panel residence time. Therefore, the contamination-free process criterion in Eq. 9 represents a conservative limit for these contaminants.

Both solution kinematic viscosity and hole aspect ratio greatly influence panel motion requirements for contamination-free processing, Figures 13 and 14. For constant-aspect-ratio product, typical process solution chemistries have viscosity ranges that necessitate panel movement parameters which vary by a factor of 2.9, Table 1. In manufacturing applications with a programmable hoist system, the individual panel agitation parameters can be implemented for each process chemistry. For mechanical movement systems with a common drive mechanism, all process tanks must utilize the panel agitation requirements for the highest viscosity chemistry. When feasible, reduc-

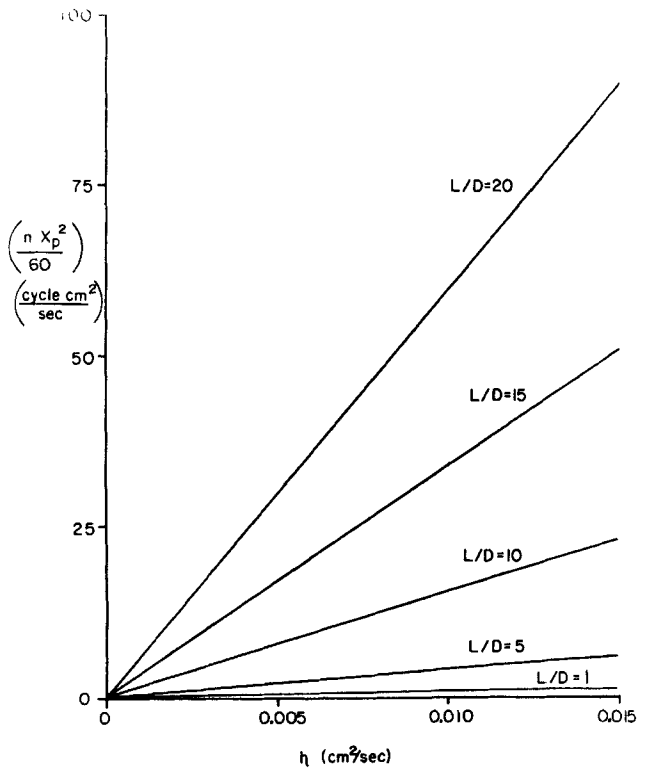

Figure 13. Minimum panel movement requirements for contamination-free processing.

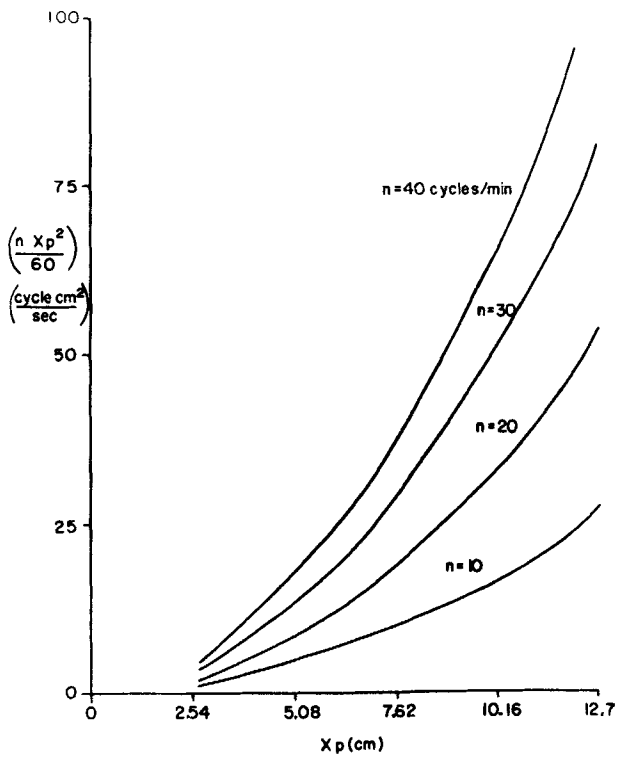

Figure 14. Breakdown of panel movement requirements into displacement rates and stroke lengths.

tion of panel movement is achievable from decreased solution viscosities at higher bath operating temperature. As an example, the panel velocity for water rinse tanks is decreased approximately 30% by an operating temperature increase of 50 K above room temperature (298 K).

In the laminar flow regime of hydrodynamic model applicability, contamination-free hole processing is independent of the absolute magnitude of the panel thickness or hole diameter, Eq. 9. Only the aspect ratio of the hole affects panel movement parameters. High-aspect-ratio holes approach the limits of mechanical panel movement as an effective method for imparting hole solution flow, Figures 13 and 14. Experience indicates that panel cycle rates far beyond 30–35 cycle/min are not acceptable in open-tank systems due to significant surface splashing and solution spillage. Long panel strokes are not favorable since the process loading (panel production/tank volume) is lessened.

Fast chemical process concerns arise when inadequate mass and momentum solution transport in holes can seriously affect the process effectiveness. A typical example is burnt or powdery deposits caused by copper electroplating at high rates with insufficient fluid flow. Copper electroplating in plated through-holes has been extensively studied both theoretically and experimentally (Alkire and Mirarefi, 1973; Kessler and Alkire, 1976 a, b; Engelmaier and Kessler, 1978). Kessler and Alkire provided an electrochemical model to predict minimum solution hole velocities for high-quality copper electrodeposits from

$$V_H \geq \frac{C_1 J^3 DL}{D_i^2 C_c^3} \tag{10}$$

where J is the average current density, D_i is the diffusion coefficient, and C_C is the bulk copper concentration. Minimal panel

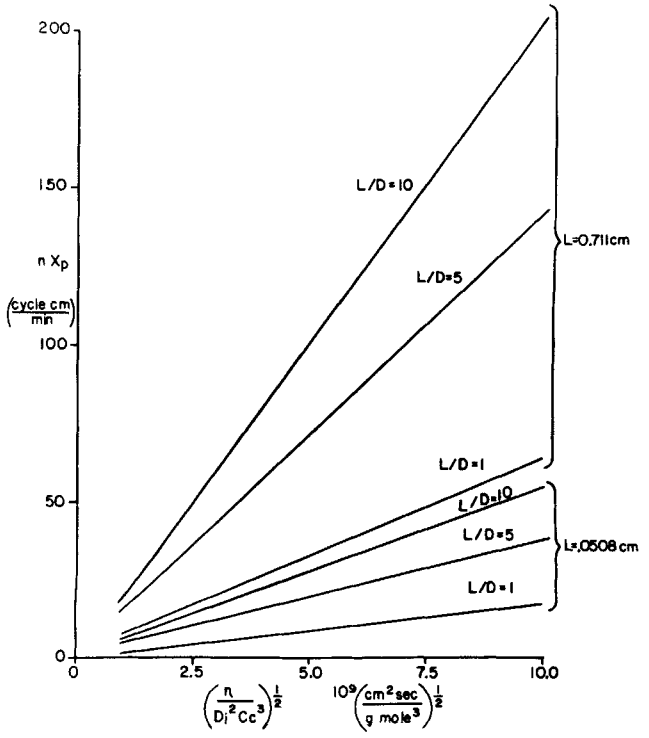

Figure 15. Minimum panel movement requirements for quality copper electroplating.
$J = 0.010$ A/cm^2

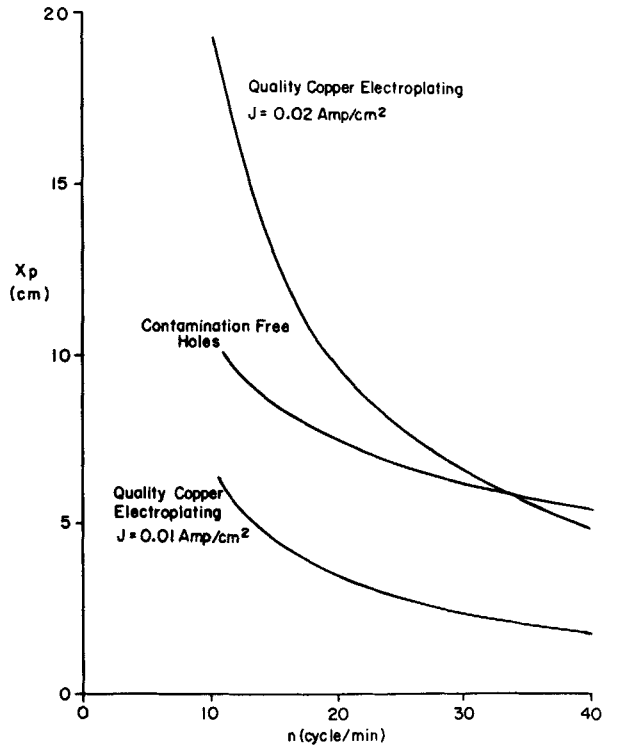

Figure 16. Panel movement requirements for quality copper electroplating with no contamination effects.
$D = 0.0457$ cm; $L/D = 8.3$; $(\eta/D_i^2 C_c^3)^{1/2} = 4.53 \times 10^9$

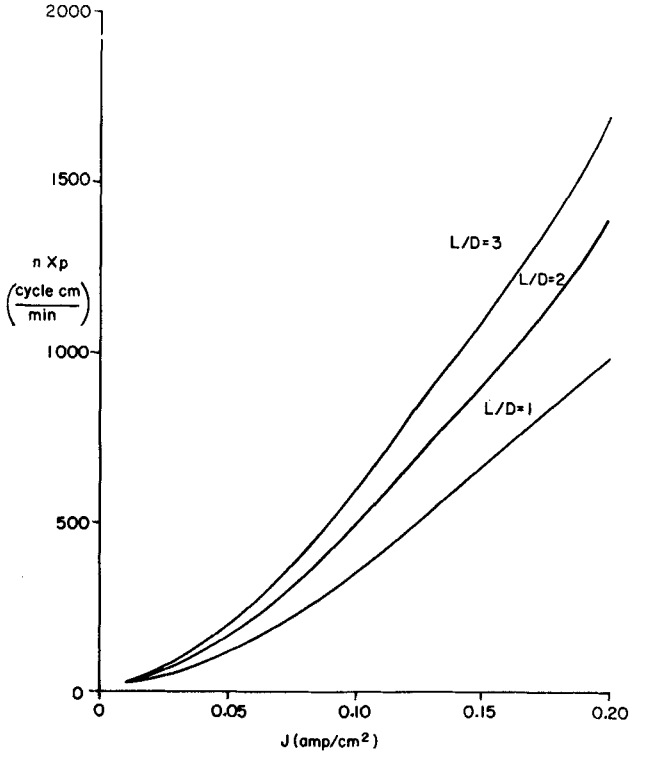

Figure 17. Effect of current density on panel movement requirements for quality copper electroplating.
$L = 0.102$ cm; $(\eta/D_i^2 C_c^3)^{1/2} = 4.53 \times 10^9$

movement parameters are defined by application of the hydrodynamic model to this flow criterion, yielding

$$nX_p \geq \left[\frac{C_2 \eta J^3}{D_i^2 C_c^3}\left(\frac{L}{D}\right) L\right]^{1/2} \tag{11}$$

This criterion represents an additional panel movement requirement supplementing the contamination-free process constraint.

At set solution chemistry, panel movement demands for high-quality copper electroplating depend on current density, panel thickness, and hole aspect ratio, Figure 15. For a hole of given geometry, the panel movement is controlled by the plating current density, Figure 16. At low current densities, contamination-free processing concerns determine the panel movement parameters. At high current densities the high-quality copper deposit criterion sets the required agitation.

Due to resistive heating in solution and high cupric ion concentrations, copper electroplating solutions can have significant natural convection effects that contribute to hole solution flow. Literature studies (Engelmaier and Kessler, 1978; Alkire and Mirarefi, 1977) suggest hole solution flows as high as 1.7 cm/s are observed for concentrated copper solutions in large-diameter holes. This additional solution transport reduces the flow requirements for mechanical panel movement. As a result, panel movement predictions are conservative for copper electroplating solutions. Still, the limits of reciprocating panel movement as an effective method for hole solution transport are evident for high current density plating of low-aspect-ratio product, Figure 17.

Acknowledgment

The authors wish to thank W. Pimbley for insight and guidance in development of the fluid flow model; C. Gazdik for aid in performing flow visualization studies; T. Connor and M. Pond for aid in performing shear stress measurements; S. Pisani for cross-section analytical skills; and the University of Illinois for the use of current-follower equipment.

Notation

C_B = bulk concentration of ferricyanide ion, gmol/cm^3
C_C = bulk concentration of cupric ion, gmol/cm^3
C_D = drag coefficient
C_1, C_2 = constants, (gmol/Coul)^3
D = hole diameter, cm
D_i = diffusion coefficient, cm^2/s
F = Faraday's constant, 96,500 Coul/g equiv
i_L = limiting current density, Amp/cm^2
J = current density, Amp/cm^2
K = mass transfer coefficient, cm/s
L = panel thickness, cm
L_E = electrode length in flow direction, cm
L_P = panel length, cm
N_H = number of holes per panel
$(N_R)_P$ = Reynolds number for flow around panel
$(N_R)_H$ = hole Reynolds number
n = panel cycle rate, cycle/min
n_E = number of electrons in charge transfer, g equiv/gmol
ΔP_H = hole pressure drop, g/cm · s^2
ΔP_P = pressure drop across panel, g/cm · s^2
Q_H = volumetric solution flow in holes, cm^3/s
Q_P = volumetric solution flow around panel edges, cm^3/s
Sc = Schmidt number
T = temperature, K
V_H = solution velocity in hole, cm/s
V_P = panel velocity, cm/s
W_P = panel width, cm
X_H = solution displacement in hole, cm/s
X_P = panel displacement in one direction, cm
τ_w = shear stress at wall, g/cm · s^2
η = solution kinematic viscosity, cm^2/s
ρ = solution density, g/cm^3
μ = solution viscosity, g/cm · s

Literature cited

Alkire, R., and W. Chen, "High-Speed Selective Electroplating with Single Circular Jets," *J. Electrochem. Soc.*, 2424 (Nov., 1982).
Alkire, R., and A. Mirarefi, "Current Distribution within Tubular Electrodes Under Laminar Flow," *J. Electrochem. Soc.*, 1507 (Nov., 1973).
———, "Current Distribution in a Tubular Electrode Under Laminar Flow; One Electrode Reaction," *J. Electrochem. Soc.*, 1043 (July, 1977).
Binder, R., *Fluid Mechanics*, Prentice-Hall, Engelwood Cliffs, NJ (1959).
Bird, R., W. Stewart, and E. Lightfoot, *Transport Phenomena*, Wiley, New York, 107–108 (1960).
Dimopoulos, H., and T. Hanratty, "Velocity Gradients at the Wall for Flow Around a Cylinder for Reynolds Numbers between 60 and 360," *J. Fluid. Mech.*, **33**, Pt. 2, 303 (1968).
Eisher F., "Das Widerstandsproblem," *Proc. 3rd Int. Cong. Appl. Mach.*, Stockholm (1981).
Engelmaier W., and T. Kessler, "Investigation of Agitation Effects on Electroplated Copper in Multilayer Board Plated Through-Holes in a Forced Flow Plating Cell, *J. Electrochem. Soc.*, p. 36 (Jan., 1978).
Haak, R., C. Odgen, and D. Tench, "Evaluation of Agitation within Circuit Board Through-Holes," *J. Appl. Electrochem.*, 771 (1981).
Hanratty T., and J. Campbell, "Measurement of Wall Shear Stress," *Fluid Mechanics Measurements*, Hemisphere, 572 (1983).
Heikkla, K., L. Whitney, G. Peterson, and R. Pylkki, "Factors Affecting Through-Hole Plating of Printed Wiring Boards," *Electronic Packaging and Production*, p. 29 (Sept., 1984).
Ju, J. B., "High-Speed Impinging Jet Plating: Slot Jet and Through-Hole Plating," Ph.D. Diss., Univ. Illinois (1984).
Kessler, T., and R. Alkire, "A Model for Copper Electroplating of Multilayer Printed Wiring Boards," *J. Electrochm. Soc.*, 990 (July, 1976).
———, "Copper Plating of Multilayer Printed Wiring Boards," *Plating and Surface Finishing*, p. 22 (Sept., 1976).
Langhaar, H., "Steady Flow in the Transition Length of a Straight Tube," *J. Appl. Mech.*, **64**, 52 (1942).
Malak, T., "Acid Copper Plating of Printed Circuits," *Products Finishing*, p. 38 (Mar., 1981).
McCabe W., and J. Smith, *Unit Operations of Chemical Engineering*, McGraw-Hill, New York, pp. 84–91 (1957).
Muzushina T., "Application of Shear Stress Measurements," *Advances in Heat Transfer*, **7**, Academic Press, 136 (1971).
Pimbley, W., "Liquid Flow Through an Ink Jet Nozzle," IBM Tech. Rept. TR 01.2494 (Aug., 1982).
Schering/Chemcut Corp., *PTH Processes Technical Data Sheets*. State College, PA (1981).
Selman, J., and C. Tobias, "Mass Transfer Measurements by the Limiting Current Technique," *Advances in Chemical Engineering*, **10**, Academic Press, p. 217, (1978).
Tidwell, L., T. O'Keefe, V. Ettel, and D. Robinson, "Unit Processes in Extractive Metallurgy: Electrometallurgy," Am. Electroplater's and Surface Finishers Soc. Short Course Notes, p. 3.3.7. (1981).

Manuscript received July 25, 1986, and revision received Nov. 21, 1986.